Plant model and control algorithm development for torque ripple compensation of PMSMs

Master's thesis in Electric Power Engineering

Xudong Wang

DEPARTMENT OF Electrical Engineering

CHALMERS UNIVERSITY OF TECHNOLOGY
Gothenburg, Sweden 2021
www.chalmers.se

Master's thesis 2021

Plant model and control algorithm development for torque ripple compensation of PMSMs

Xudong Wang

CHALMERS
UNIVERSITY OF TECHNOLOGY

Department of Electrical Engineering
Division of Electric Power Engineering
Chalmers University of Technology
Gothenburg, Sweden 2021

Plant model and control algorithm developmentfor torque ripple compensation of PMSMs
NAME FAMILYNAME

Supervisor: Jonas Ottosson, Sebastian Hall, Volvo Group
Examiner: Torbjörn Thiringer, Department of Electrical Engineering

Master's Thesis 2021
Department of Electrical Engineering
Division of Electric Power Engineering
Chalmers University of Technology
SE-412 96 Gothenburg
Telephone +46 31 772 1000

Typeset in LaTeX
Printed by Chalmers Reproservice
Gothenburg, Sweden 2021

Plant model and control algorithm development for torque ripple compensation of PMSMs
Xudong Wang
Department of Electric Power Engineering
Chalmers University of Technology

Abstract

This thesis investigates torque ripple in a permanent-magnet synchronous motor (PMSM). Firstly, a PMSM model is developed with spatial harmonics and saturation, which is based on Finite Element Method (FEM) with the help of a Python based open-source software PYLEECAN. Then the results are converted into look-up tables and applied to an existing electric drive system in Simulink. The existing controller performances will be evaluated. Finally, a torque ripple compensation is realized and its effectiveness is evaluated.

Keywords: PMSM, torque ripple compensation, FEM, FOC.

Acknowledgements

I would like to first express my sincere appreciation to supervisors Dr. Jonas Ottosson and Dr. Sebastian Hall at Volvo Group, for their invaluable insights, encouragement and support. Their enthusiasm, knowledge and creativity inspire me much during the thesis and in later professional life.

Also, I greatly appreciate my examiner Dr. Torbjörn Thiringer at Chalmers University of Technology, for his crucial feedback, patience and guidance on the project and report.

Many thanks to Dr. Andersson Rasmus at Volvo Group, for his crucial help on the machine FEM simulation. I'm fortunate to have been part of Department of Motor Drive System Control at Volvo Group, which has a very professional atmosphere and kind colleagues. At last, I'm very grateful to my family and friends with their love and support.

Xudong Wang, Gothenburg, Aug 2021

Contents

1

Introduction

1.1 Motivation and background

Permanent magnet synchronous motors (PMSMs) are of high demand for electric vehicles due their good dynamic performance, high efficiency and high power density. In PMSMs, torque ripple, which leads to acoustic noise, mechanical vibrations and reduces the machine life time, is a critical issue[1]. Therefore, a good torque-ripple reduction strategy can improve the driving experience and the lifetime of an electric vehicle significantly

Torque ripple reduction can be realized during either the machine design or machine drive control. For a machine design approach, researchers optimize the shape and structure of PMSMs with skewing, magnet sizing or adjusting slots per poles ratio[2][3][4]. However, even if a PMSM is well designed, the torque ripple is still inevitable due to different operation and imperfect manufacturing. Thus this thesis focus on the drive control compensation development from a provided machine.

It is vital to include the torque ripple harmonic information in the PMSM model to develop the compensation control algorithm. The modeling and understanding of a high fidelity model can both facilitate the design and validation of the torque ripple reduction control. There are several ways to build such a plant model and a numerical analysis method of finite-element-method (FEM) has drawn much attention.

However, the FEM algorithm is complicated to implement for solving a partial differential equation. It is even more difficult when dealing with the complex machine geometry and multiple materials inside. Several FEM softwares have been developed for machine modelling. Some of them are user unfriendly and time consuming. Some other are commercial software and not an open-source tool.

When it comes to the PMSM drive system, the field-oriented-control (FOC) is adopted, which treats the PMSM plant model as a decoupled first order system in a dq coordinate system. However, the existing FOC control system is unable to handle the torque harmonics, and a compensation algorithm needs to be developed to optimize the control performance.

Therefore in this thesis, a Python-based FEM simulation approach is developed, which make it convenient to set up the machine and operation points. The FEM results can also be import to the PMSM drive system as a plant model in Simulink. Based on the developed plant model, the compensation algorithm is added to the conventional FOC system to reduce the torque ripples.

1.2 Previous work

1.2.1 PMSM modeling approach

The linear model of PMSM can be built in Simulink using transfer function. It's beneficial for its easier implementation. However, the linear model misses some information like the spatial harmonic. The linear model also assumes the PMSM inductance as constant, which is inaccurate due to the flux saturation.

Thus, many researchers develop the PMSM model in FEM using some commercial software of Ansys Maxwell. An open-source software of Finite Element Method Magnetics (FEMM) is also adopted in some companies. The FEMM can build the model manually or programmed using Lua, which is a lightweight programming language primarily for embedded applications.

1.2.2 Torque compensation method

Based on the prvious analysis, the current references in the current loop need to be designed to compensate the torque harmonics.

Conventionally, the PMSM drive system uses FOC with cascaded PI control loops. However, traditional PI controller has bandwidth limitation to track relatively high-frequency components in the torque ripple, which increases with speed[5]. From the 1990's, several methods have been proposed to solve this problem.

A group of papers introduce different control methods for a high control bandwidth. In [5] and [6], the authors adds additional repetitive control(REP) and Iterative learning control (ILC) block to a PI controller, utilizing the inherently periodicity of torque-ripple disturbance. [7] uses a combination of a deadbeat current controller and a current predictor appears as an appropriate approach to deal with the bandwidth limitation. These methods involve heavy computations, so their applicability is limited in transient state because it is difficult to timely update the stator current[8].

Another group of papers treat it as an optimization problem, i.e. by solving the optimum reference current with respect to the minimum torque ripples. In [8], the authors derive an analytical model of torque ripples, then construct an objective function of minimal torque ripples and losses to obtain the optimal reference current problem. In [1], model predictive control (MPC) is adopted to reduce the electromagnetic torque and feed-forward compensation used for cogging torque. In [9], multiple reference frame (MRF) analysis is used to obtain optimal currents and adaptive notch filter (ANF) is used to extract harmonics from currents. For these methods, the parameter variation should be considered because they can cause errors in the optimization problem.

1.3 Purpose of the thesis

The main purpose of this thesis is to develop a high fidelity PMSM model representing the torque ripples based on FEM. It's realized by the Python programming based on the open-source packages of PYLEECAN and a software of FEMM.

The second purpose is to implement a compensation method based on the developed model. The FEM results are implemented into Simulink to establish a PMSM plant model with a FOC drive system. Based on them, a straightforward compensation method is implemented and verified.

2

PMSM Plant Models

This chapter describes a PMSM plant model based on FEM, which include a average rotor position model and a model with spatial harmonics. A Python-based FEM simulation approach is adopted coupling with several open source software. Then different operating points are performed and output data is processed. Finally the models are export in a form of look-up tables.

2.1 Introduction to the PMSM modelling

It's important to obtain a PMSM model for machine design and control. Based on the model, it's possible to investigate the concerned machine properties like torque and magnetic flux at different operating points. Moreover, the control system can also be implemented and verified.

2.1.1 Coordinate systems for PMSM modelling

The PMSM works in the ABC three-phase coordinate system with modulated voltages, making it hard to analyze and model. It can be simplified by converting the stationary three-phase coordinate system to a rotating two-phase frame. An DQz transformation is applied to model the system in the dq-frame, which is a two-phase system rotating in a counter-clockwise direction.

The DQz transformation is performed by multiplying a transformation matrix P to the variables in the ABC-frame, given as

$$\begin{bmatrix} D \\ Q \\ Z \end{bmatrix} = P \begin{bmatrix} A \\ B \\ C \end{bmatrix} \tag{2.1}$$

The matrix P is given by

$$P = K \begin{bmatrix} cos(\theta) & cos(\theta - \frac{2\pi}{3}) & cos(\theta + \frac{2\pi}{3}) \\ sin(\theta) & sin(\theta - \frac{2\pi}{3}) & sin(\theta + \frac{2\pi}{3}) \\ \frac{1}{2} & \frac{1}{2} & \frac{1}{2} \end{bmatrix} \tag{2.2}$$

where coefficient K determines transformed variable amplitude. K is$\sqrt{\frac{2}{3}}$ for the power invariant and is $\frac{2}{3}$ for the amplitude invariant transformation. For the matrix P in (2.2), the d-axis is in alignment with phase A after transformation.

2.1.2 Models with different fidelity levels

Three different fidelity levels of a PMSM model are considered in this thesis. The first level is an analytical model, which has a linear characteristic because inductance is assumed constant without considering saturation in different current levels and temperatures.

The second and the third level models adopt a numerical method of FEM. The second level takes the magnetic nonlinear saturation into consideration and the flux has a nonlinear relationship with the currents. The third level also considers the spatial harmonics, which results from the stator tooth and the rotor positions.

In the following sections, an analytical model is first developed, and then the general FEM process for a PMSM is introduced. Finally a detailed programming-based FEM approach is described to build the second and the third level models.

2.2 Analytical model of PMSM

2.2.1 General analytical model derivation

The ideal working principle for a PMSM is that the the stator currents generate a rotating magnetic flux field with a constant amplitude, which attracts the permanent magnets in the rotor to rotate accordingly. The key to generate such a rotating magnetic flux is to create a rotating stator currents. It can be realized by three-phase balanced sinusoidal voltages v_a, v_b, v_c with a phase shift of $2\pi/3$,

$$\begin{aligned} v_a &= V_o sin(\omega t) \\ v_b &= V_o sin(\omega t - 2\pi/3) \\ v_c &= V_o sin(\omega t + 2\pi/3) \end{aligned} \tag{2.3}$$

where ω is the PMSM rotor electrical angular speed, and V_o is the input voltage peak value.

The three phase windings ABC also need to be distributed individually around the stator circumference with a $2\pi/3$ electrical space interval. The phase B winding needs to be counterclockwise away from phase A to make sure that the field is rotating in the positive direction. Thus, the sum of the three-phase input voltage v_s is given as

$$\begin{aligned} v_s &= v_a + v_b e^{j2\pi/3} + v_c e^{-j2\pi/3} \\ &= \frac{V_o}{2}[(e^{j\omega t} + e^{-j\omega t}) + (e^{j\omega t - 2\pi/3} + e^{-j\omega t - 2\pi/3})e^{j2\pi/3} + (e^{j\omega t + 2\pi/3} + e^{-j\omega t + 2\pi/3})e^{-j2\pi/3}] \\ &= \frac{3V_o}{2}e^{j\omega t} \end{aligned} \tag{2.4}$$

The result indicates that v_s is a rotating vector with the electrical speed and the $\frac{3}{2}$ times amplitude. In the abc-frame, the voltage equation is given as

$$\begin{bmatrix} v_a \\ v_b \\ v_c \end{bmatrix} = R_s \begin{bmatrix} i_a \\ i_b \\ i_c \end{bmatrix} + d \begin{bmatrix} \Psi_a \\ \Psi_b \\ \Psi_c \end{bmatrix} /dt \tag{2.5}$$

where i_a, i_b, i_c are the stator three-phase currents, R_s is the stator resistance, and Ψ_a, Ψ_b, Ψ_c are the flux linkages in the windings. The three-phase flux linkages are complex to calculate due to the mutual inductance between each phase. It can be simplified by treating the fields as a rotating space vector. Thus, the stator voltage is described by the vector

$$\boldsymbol{v_s} = K \frac{3V_o}{2} e^{j(\omega t + \theta_v)} \tag{2.6}$$

where K is the coefficient factor, and θ_v is the voltage vector initial angle. The space vector can be expressed in a two-dimension coordinate system according to the Euler's formula, which is the reason to use the Clarke transformation. Thus, the voltage in the $\alpha\beta$-frame is denoted as u_α, u_β. K is equal to $\frac{2}{3}$ for the amplitude invariant transformation because the vector's amplitude becomes $\frac{3}{2}$ times of V_o after the transformation. Similarly, the stator current and flux linkage can also be expressed in vectors of $\boldsymbol{i_s}, \boldsymbol{\Psi_s}$ with amplitude invariant as

$$\begin{aligned} \boldsymbol{i_s} &= I_0 e^{j(\omega t + \theta_i)} \\ \boldsymbol{\Psi_s} &= \Psi_0 e^{j(\omega t + \theta_\Psi)} \end{aligned} \tag{2.7}$$

where θ_i and θ_Ψ are the initial angles for current and flux linkage. Using these vectors, the flux linkage derivative is simplified in the voltage equation as

$$\boldsymbol{v}_s = R_s \boldsymbol{i}_s + \frac{d\boldsymbol{\Psi}_s}{dt} = R_s \boldsymbol{i}_s + j\omega \boldsymbol{\Psi}_s \tag{2.8}$$

To calculate the power in the $\alpha\beta$-frame, a coefficient K_p is added to make it equivalent to the power in the *abc*-frame

$$K_p \begin{bmatrix} u_\alpha \\ u_\beta \end{bmatrix}^T \begin{bmatrix} i_\alpha \\ i_\beta \end{bmatrix} = \begin{bmatrix} u_a \\ u_b \\ u_c \end{bmatrix}^T \begin{bmatrix} i_a \\ i_b \\ i_c \end{bmatrix} \tag{2.9}$$

K_p is solved as $\frac{3}{2}$ after applying the Clarke transformation.

Thus the active power P_e is given by

$$\begin{aligned} P_e &= K_p Re\{\boldsymbol{v}_s \cdot \boldsymbol{i^*}_s\} \\ &= \frac{3}{2} Re\{j\omega_e \boldsymbol{\Psi}_s \cdot \boldsymbol{i^*}_s\} \\ &= \frac{3}{2} Re\{j\omega_e \Psi_0 I_0 e^{j(\theta_{Psi} - \theta_i)}\} \\ &= -\frac{3}{2} \omega_e \Psi_0 I_0 sin(\theta_{Psi} - \theta_i) \\ &= \frac{3}{2} \omega_e Im\{\boldsymbol{\Psi^*}_s \cdot \boldsymbol{i}_s\} \end{aligned} \tag{2.10}$$

where the resisitive loss is neglected. Thus, the electromagnetic torque T_e is given as

$$\boldsymbol{T_e} = \frac{3}{2}\frac{P_e}{\omega_n} = \frac{3}{2}p \cdot Im\{\boldsymbol{\Psi^*}_s \cdot \boldsymbol{i}_s\} \tag{2.11}$$

where p is the machine pole pair number, ω_n is the mechanical speed.

The $\alpha\beta$-frame model is intuitive to understand but is inconvenient for calculations. To deal with it, the stationary coordinate system is transformed to a frame rotating with the same speed as the one of the field vector. The stationary direct axis is beneficial to align with the rotor magnet because the rotor permanent magnet is an independent magnetic source. Thus the dq-frame is adopted using the DQ transformation and $\boldsymbol{v}_s, \boldsymbol{\Psi}_s, \boldsymbol{i}_s$ are expressed as $v_d + jv_q, \Psi_d + j\Psi_q, i_d + ji_q$. The voltage equation is rewritten as

$$\begin{aligned} v_d + jv_q &= R_s(i_d + ji_q) + j\omega(\Psi_d + j\Psi_q) \\ &= R_s i_d - \omega\Psi_q + j(R_s i_q + \omega\Psi_d) \end{aligned} \tag{2.12}$$

The torque in (2.11) is expressed as

$$\begin{aligned} T_e &= \frac{3}{2}pIm[(\Psi_d + j\Psi_q) * (i_d + ji_q)] \\ &= \frac{3}{2}p(\Psi_d i_q - \Psi_q i_d) \end{aligned} \tag{2.13}$$

The dq-frame inductance L_d, L_q are constant in the linear model and the dq fluxes are expressed as

$$\begin{aligned} \Psi_d &= \Psi_m + L_d i_d \\ \Psi_q &= L_q i_q \end{aligned} \tag{2.14}$$

where Ψ_m is the no-load flux linkage from the rotor permanent magnets. Thus, the dq voltages are

$$\begin{aligned} v_d &= R_s i_d - \omega L_q i_q \\ v_q &= R_s i_q + \omega(\Psi_m + L_d i_d) \end{aligned} \tag{2.15}$$

The torque is

$$\begin{aligned} T_e &= \frac{3}{2}p[(\Psi_m + L_d i_d)i_q - L_q i_q i_d] \\ &= \frac{3}{2}p[\Psi_m i_q + (L_d - L_q)i_d i_q] \end{aligned} \tag{2.16}$$

2.2.2 Torque ripple analysis

There are multiple reasons causing the torque ripple like harmonics in magnetic flux, cogging torque, inductance variation due to magnetic saturation, and the current measurement errors[8][10]. This thesis focuses on the flux harmonics and the cogging torque.

2.2.2.1 Flux harmonics

Considering the flux harmonics Ψ_{dhar}, Ψ_{qhar} in the dq-axis fluxes Ψ_d, Ψ_q

$$\begin{aligned} \Psi_d &= \Psi_m + L_d i_d + \Psi_{dhar} \\ \Psi_q &= L_q i_q + \Psi_{qhar} \end{aligned} \tag{2.17}$$

The electromagnetic torque T_e in (2.16) is rewritten as

$$\begin{aligned} T_{em} &= \frac{3P}{4}(\Psi_d i_q - \Psi_q i_d) \\ &= \frac{3P}{4}\{\Psi_m i_q + (L_d - L_q) i_d i_q + (\Psi_{dhar} i_q - \Psi_{qhar} i_d)\} \end{aligned} \tag{2.18}$$

By applying Fourier analysis, the flux in the abc frame contains only the odd order harmonics, due to its symmetry property in the machine mechanical space. Additionally, the 3rd and its multiples harmonics don't exist since they are eliminated in the three-balanced machine system. After the DQz transformation, the fluxes in the dq frame contain the harmonics orders of the multiples of six, such as the 6th and the 12th, which are represented by the 5th, 7th, 11th and 13th harmonics in the abc frame.

2.2.2.2 Cooging torque

The cogging torque comes from the existence of the slots in the stator of the machine. It is the result of the interaction of the permanent magnets in the rotor and the changing of the stator reluctance[8]. It could be obtained from both analytical calculation and FEM simulations. The cogging torque can be obtained both from theory and the numerical method of FEM. By setting the input current $i_a = i_b = i_c = 0$ in the FEM software, the output torque result is the cogging torque.

2.3 The high-fidelity model in this thesis

This thesis utilizes a combination of Simulink and FEM to build the PMSM model, where FEM reflects the nonlinear characteristic parts of the machine. The FEM results are converted to look-up tables and imported into Simulink.

2.3.1 FEM introduction

In reality, the PMSM flux linkage has a nonlinear relationship with the currents due to the inductance varies for different currents. The variations can be obtained by FEM simulations. The FEM is a numerical analysis method to solve differential equations like Maxwell's equations, and is widely used in electric machine design.

The general FEM process usually include the geometry modeling, boundary conditions, meshing, material conditions, excitation and initial conditions. FEM can be realized with the help of softwares like Ansys, MATLAB and FEMM.

The machine geometry is defined including dimensions and winding. Different materials are applied to the corresponding parts in the machine and their properties are defined. The operating points are set for the feasible dq-axis currents and rotor positions. The discretization steps are also picked in considerations of accuracy and calculation cost. The above settings are configured in programming scripts, making it easier to check, modify and set up a batch of simulations for different inputs.

2.3.2 Plant model overview

Figure 2.1 shows a discrete PMSM plant model in the dq-frame without rotor position dependence.The input to the electro-magnetic part of the model are voltages and rotor angular frequency, the internal states are fluxes and the output are currents. The input to the mechanical part of the model is the torque from the EM and an external load torque and the output is the electrical angular frequency. The fluxes in the dq-frame are calculated from integration of the induced voltages and the resistive voltage drop as

$$\psi_d[n] = \psi_d[n-1] + T_s(v_d[n] - R_s i_d[n-1] + \omega[n-1]\psi_q[n-1]) \tag{2.19}$$

$$\psi_q[n] = \psi_q[n-1] + T_s(v_q[n] - R_s i_q[n-1] + \omega[n-1]\psi_d[n-1]) \tag{2.20}$$

where p is the number of pole pairs. The fluxes are fed to lookup tables and the stator current is obtained. The elnectro-magnetic torque, T_e, is calculated as

$$T_e[n] = \frac{3p}{2}(\psi_d[n]i_q[n] - \psi_q[n]i_d[n]) \tag{2.21}$$

The mechanical speed, ω_m, is calculated according to

$$\omega_m[n] = \omega_m[n-1] + T_s\frac{1}{J}(T_e[n] - T_L[n] - B\omega_m[n-1]) \tag{2.22}$$

where J and B are the inertia and friction damping constant, respectively. When considering rotor position, an additional dimension of rotor position will be added to the dq current lookup tables. If temperature is also included, the lookup tables have four dimensions in total. The torque in the scheme can also be obtained from a three-dimensional lookup tables instead of equations.

The discrete equations are implemented in Simulink. The nonlinear relationships of flux to current and the torque to current are realized by the lookup tables, which are generated by FEM.The later section introduces the method to perform FEM and obtain needed lookup tables with and without spatial harmonics. The look-up tables have three dimensions of id, iq and the rotor position, where the rotor position is considered to reflect the spatial harmonics.

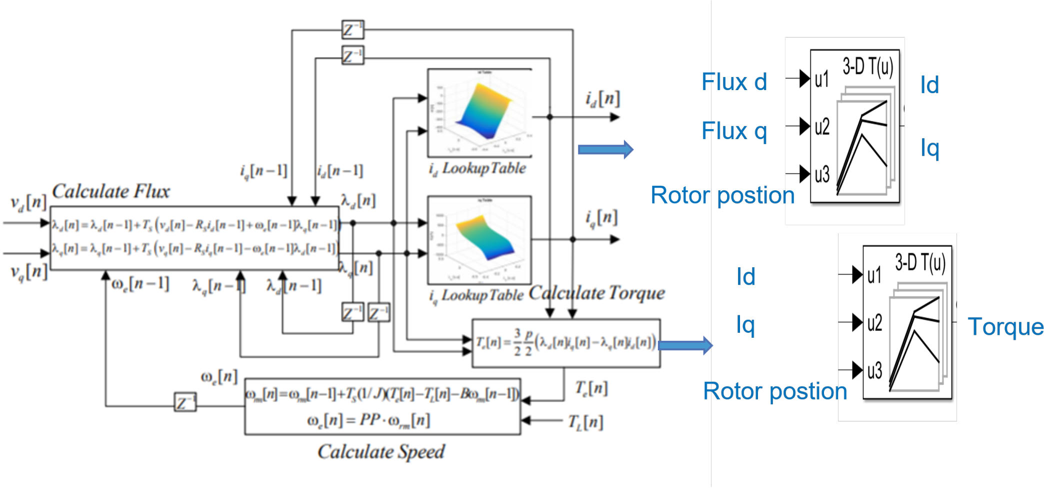

Figure 2.1: Overview of a PMSM plant model scheme with rotor sweeping

2.3.3 Workflow and platform for modeling

There are several approaches and software to perform FEM simulations for PMSMs. This thesis adopts an open source FEM software - FEMM; a Python based package - PYLEECAN; and a Python distribution - Anaconda.

FEMM is a software to solve the low frequency electromagnetic problems [11]. PYLEECAN provides a user-friendly and flexible simulation framework for the design of electrical machines and drives[12]. The coupling between PYLEECAN and FEMM enables a convenient, user-friendly and automatic way of carrying out FEM simulations through python scripts. Anaconda is a distribution of the Python programming languages for scientific computing, to simplify package management[13]. Python is coded on the Anaconda platform using the Spyder software.

The workflow to generate a model is shown in Figure 2.2. The FEM configuration and the machine definition is implemented in Python via PYLEECAN. PYLEECAN handles the connection to FEMM and carries out the FEM-calculations according to defined operating points. With FEM results from PYLEECAN, lookup tables are generated using the Python package and later applied into Simulink.

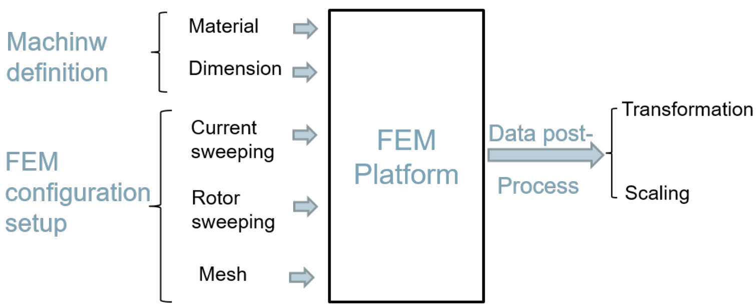

Figure 2.2: Workflow to generate PMSM model on FEM

2.4 A programming-based FEM approach

2.4.1 Machine definition

The machine dimensions and material selection are adopted from [14]. The dimensions are slightly revised using the PYLEECAN. The properties for the steel and magnet material are obtained from datasheets. The materials are temperature dependent and the magnet properties are shown in Figure 2.3 [15].

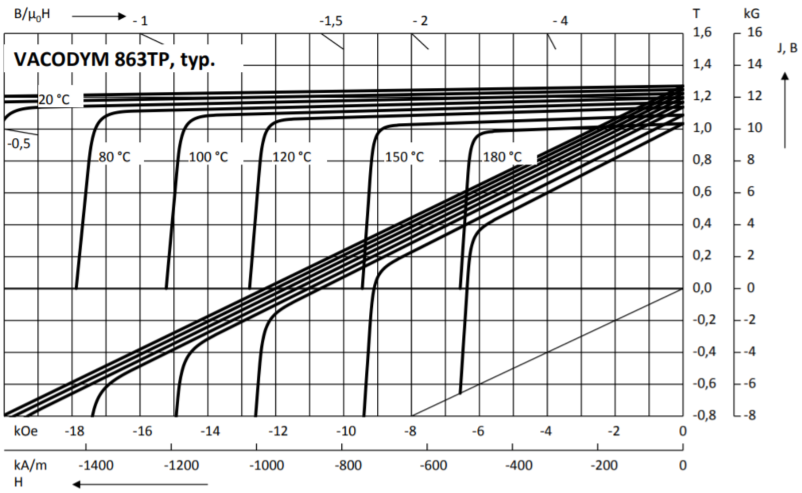

Figure 2.3: Vacodym 863 TP magnet characteristics with intrinsic and normal BH-curves for different temperatures

In PYLEECAN, a machine is constructed as an object from a pre-defined Python class, including different machine typologies like PMSM and induction machine. The lamination and the magnets are defined using either script templates or a graphical user interface (GUI). An example of what the GUI looks like can be seen in Figure 2.4. The defined machine can be saved in *.json* file, which can be imported from PYLEECAN directly for later use.

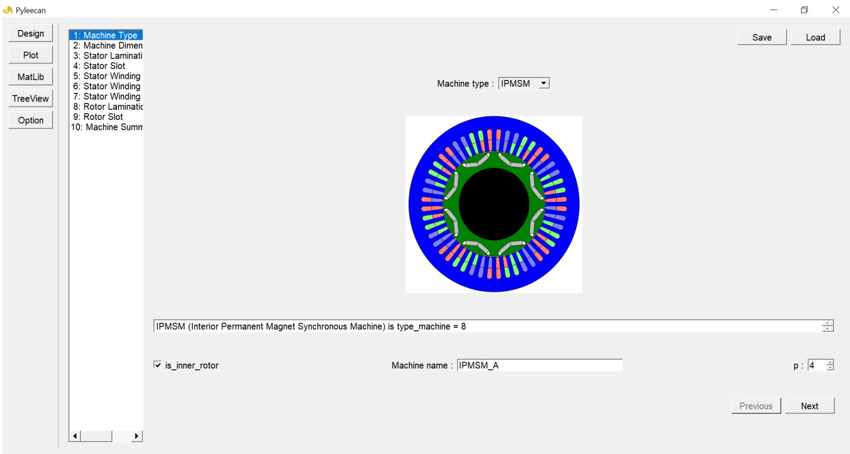

Figure 2.4: PYLEECAN GUI interface

2.4.2 Current and rotor sweeping configuration

Based on the defined machine, different operating points can be set with specific input current references and rotor speed. The default input currents are RMS values from the amplitude invariant Direct-quadrature-zero(DQZ) transformation.

PYLEECAN can automatically perform FEM for different operating points, by defining a group of desired input current references and a specific speed in a matrix. In this thesis, input currents are defined in a rectangular range as shown in Figure 2.5. D axis and q axis current references are selected from -500A to 0A and 0A to 500A for peak value with current steps of 10A, by considering the designed operating range from paper [14].

Rotor sweeping is defined by rotor speed. The angle in degree could be obtained through simulation time t in seconds and rotor speed N_0 in rpm as

$$\theta = \frac{t \cdot N_0}{60} 360 \tag{2.23}$$

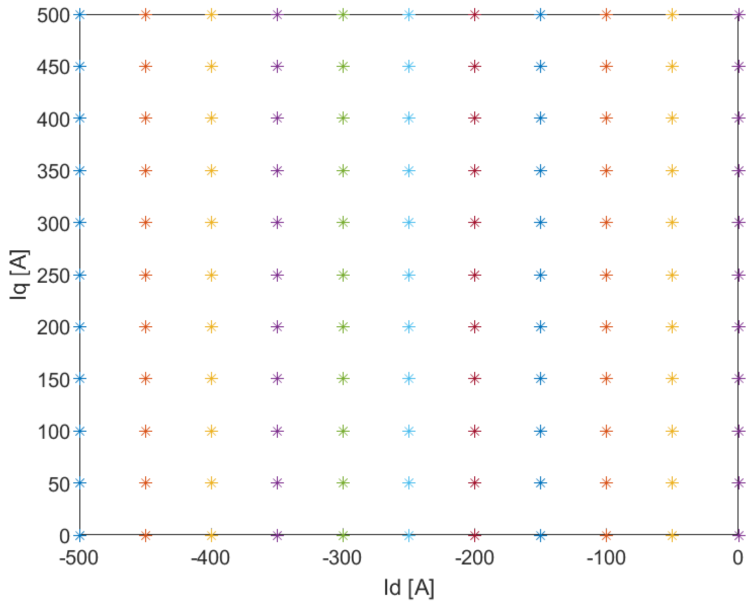

Figure 2.5: Rectangular current input

The desired outputs are the fluxes in three phase ψ_A, ψ_B, ψ_C, the electromagnetic torque T_em and the rotor angle θ. They are calculated from FEM and stored in a data structure using the ScidataTool python package. This package is beneficial for storing data in a structural way with multiple dimensions, which is convenient to plot and perform fast Fourier transform(FFT).

2.4.3 Descritization step and mesh setting

To perform FEM on PMSM, partial differential equations are solved by splitting spaces into meshes and discretizing time and circumferential space of air gap. They are optimized for a more accurate FEM model.

Meshes near the air gap are set to the smaller size because in this tiny space the flux varies more than other places in PMSM. Machine periodicity and harmonic frequency are considered for discretization. Taking the advantage of the PMSM periodicity of pole pairs can help to save much simulation time. Thus, Time and spacial steps are set to a multiple of three due to total three pole pairs in the machine. With a specific speed of 2000rpm and the dominate 6th order flux harmonics, the number of spatial discretization steps also takes the Nyquist frequency of the harmonics into account.

2.4.4 Data post processing

The FEM simulations can be performed on the software platform with the above machine definition and configurations. The results of it give a group of data lists, which are the flux and torque values in ABC-frame for different combinations of temperatures, ABC currents and rotor positions.

After the DQz transformations, it's important to consider the input and output data scaling to prevent unmatched obtained data. PYLEECAN takes the RMS value with amplitude-invariant for input current by default. Thus, flux is also subjected to the amplitude-invariant correspondingly and input dq currents are scaled with $\sqrt{2}$ for peak values.

2.5 FEM results

2.5.1 Average results without spatial harmonics

Figure 2.7, 2.6 and 2.8 show the FEM results without taking the rotor positions into account by calculating the average values over all the rotor positions. As indicated in the figures, torque and dq-fluxes saturates when dq-currents are high enough, caused by the material permeance saturation.

The d-axis flux increases as i_d decreases in negative, because the negative i_d generates an opposing flux to the rotor permanent magnet magnetic flux. The d-axis flux also changes with i_q due to the cross-saturation phenomena. The q-axis flux increases as i_q increases and the saturation appears as i_q goes higher. The torque contour also indicates the nonlinear characteristic due to the flux saturation.

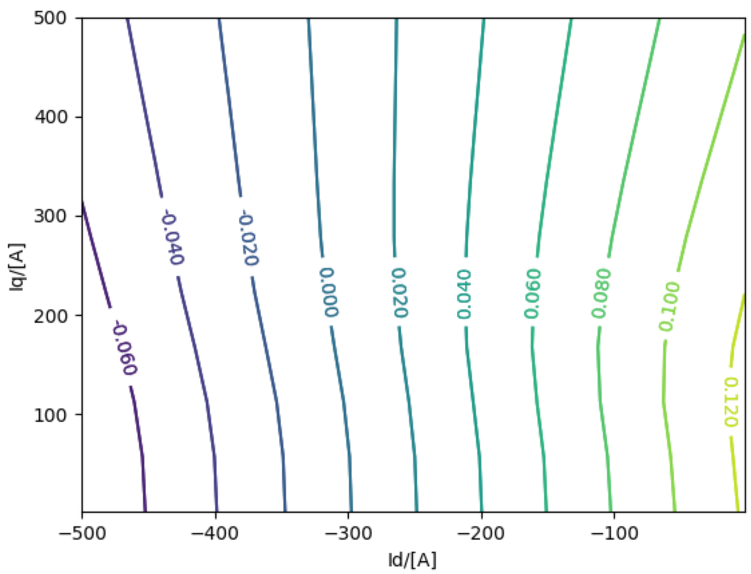

Figure 2.6: D-axis flux for different dq-currents

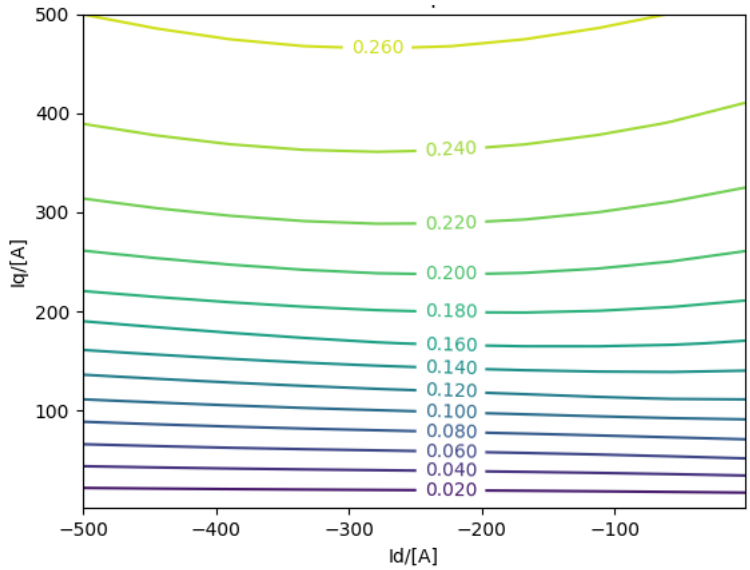

Figure 2.7: Q-axis flux for different operating points

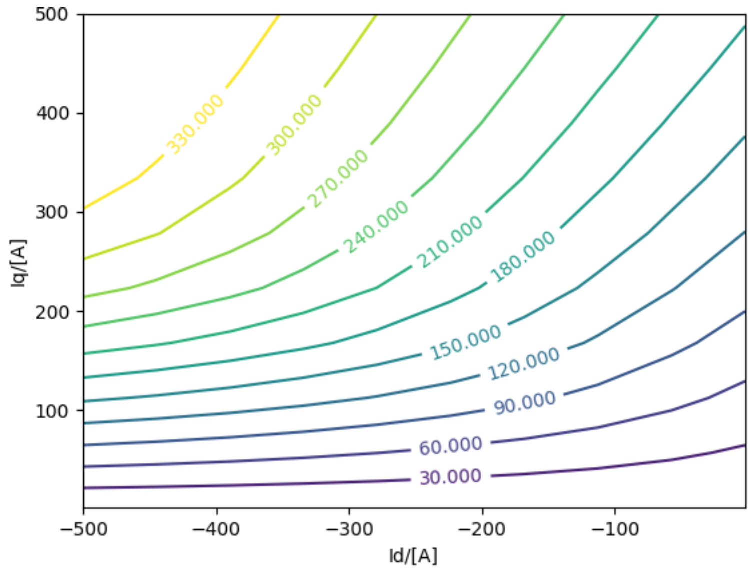

Figure 2.8: Torque for different operating points

2.5.2 Spatial harmonics at one operating point

The spatial harmonics in flux and torque are simulated at a specific operating point and compared between a high and low simulation resolution. The operating point is $I_d = -223A, I_q = 389A$ and the temperature is $20°C$. The low resolution uses 96 time steps of the whole simulation period while the high resolution uses 1800 time steps.

Figure 2.9, 2.10 and 2.11 show the spatial harmonic waveform in time domain for the dq-axis flux and torque respectively. High and low resolution results are also compared in the figures. It can seen that the low resolution has some data points missing when representing the ripples, which is worse for torque ripples.

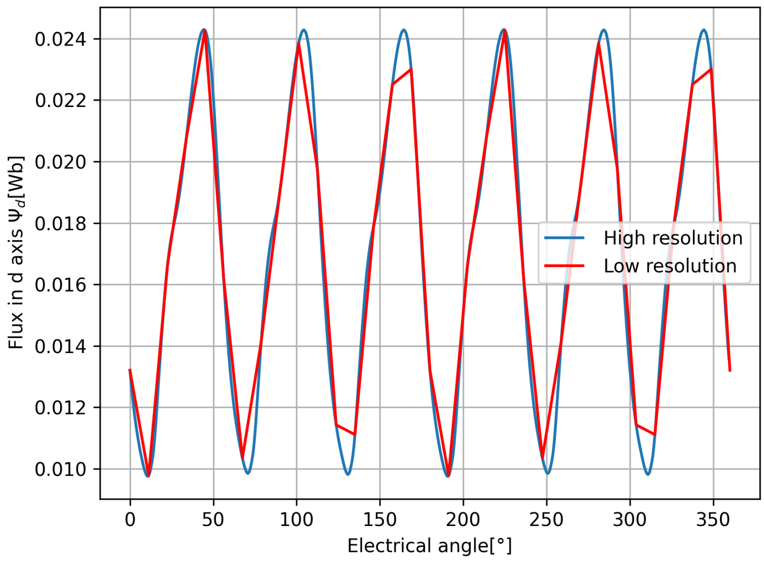

Figure 2.9: D-axis flux comparison between high and low resolution simulation

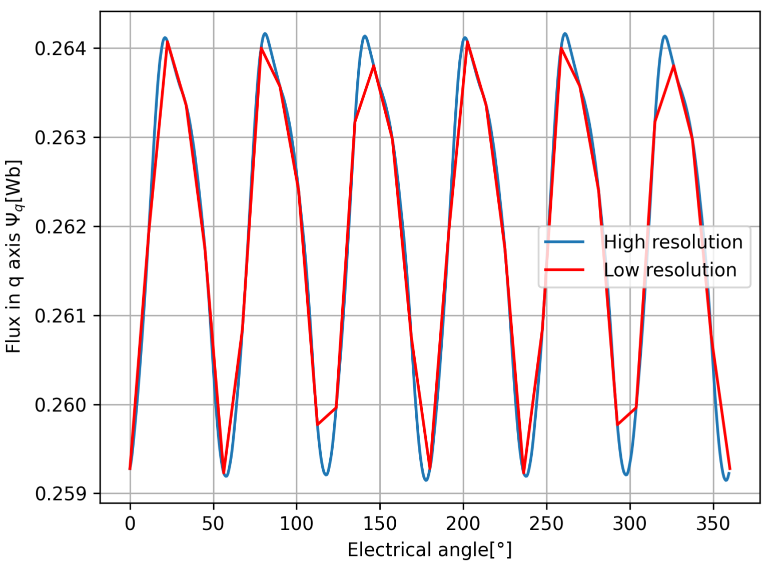

Figure 2.10: Q-axis flux comparison between high and low resolution simulation

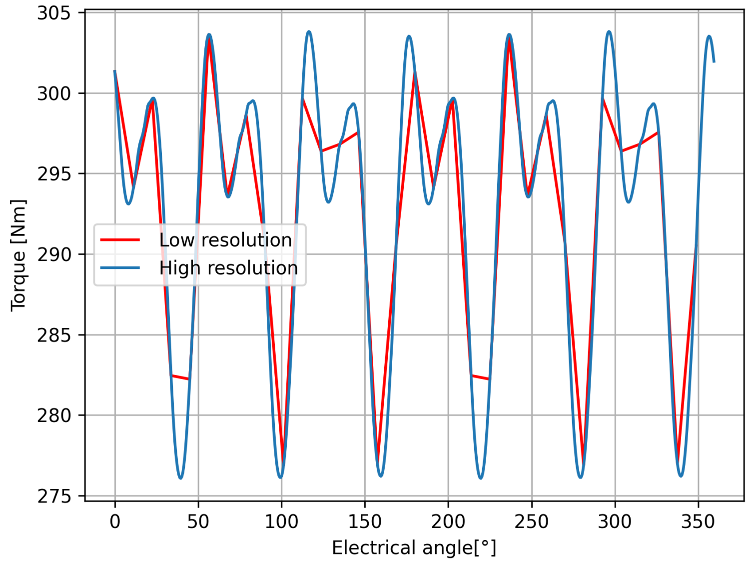

Figure 2.11: Torque harmonics comparison between high and low resolution simulation

D-axis flux FFT results are shown in Figure 2.12 and 2.13. The dominating spatial harmonic order is the 6th, as well as some other even harmonics like the 12th and 18th. The even harmonics come from the DQz transformation of the odd harmonics in the ABC frame such as the 5th, 7th and 11th etc. The low resolution FFT results exhibit almost the same magnitude for the fundamental, the 6th and the 12th harmonics but is unable to represent the higher order harmonics due to fewer sampling points.

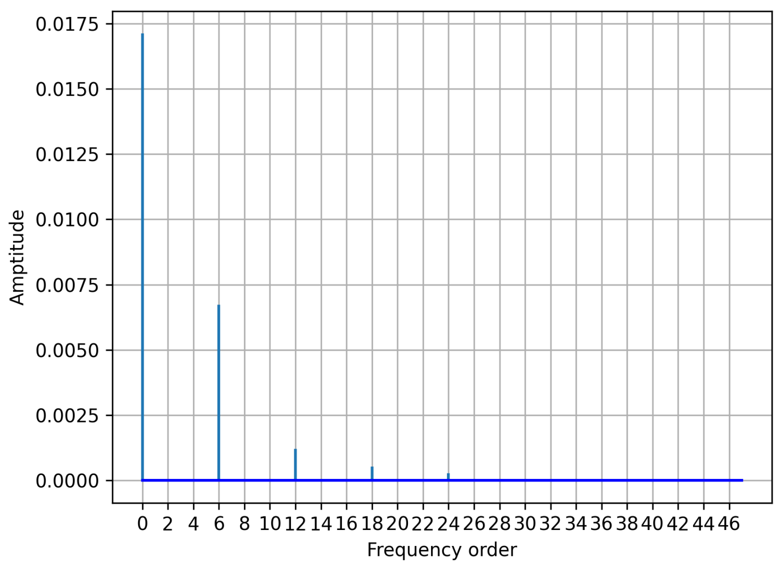

Figure 2.12: FFT for D-axis flux with high resolution

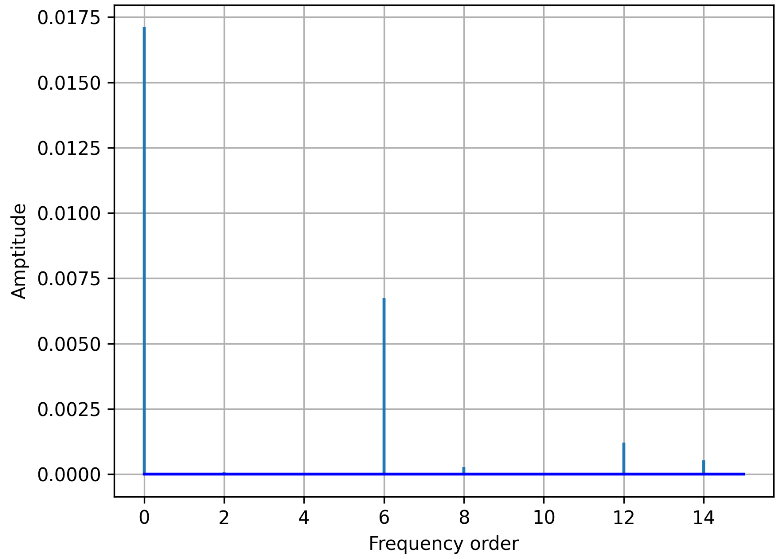

Figure 2.13: FFT for D-axis flux with low resolution

FFT results for q-axis flux are shown in Figure 2.14 and 2.15. The q-axis fundamental flux magnitude is more than 10 times of that of the d-axis at this operating point while the 6th harmonics is only the half. The 6th order harmonic is also the dominant order. The 12th, 18th and 24th harmonics are also observed. The low resolution result shows higher magnitudes for 8th and 14th harmonics compared to the high resolution since only 16 points can be calculated in the low resolution FFT.

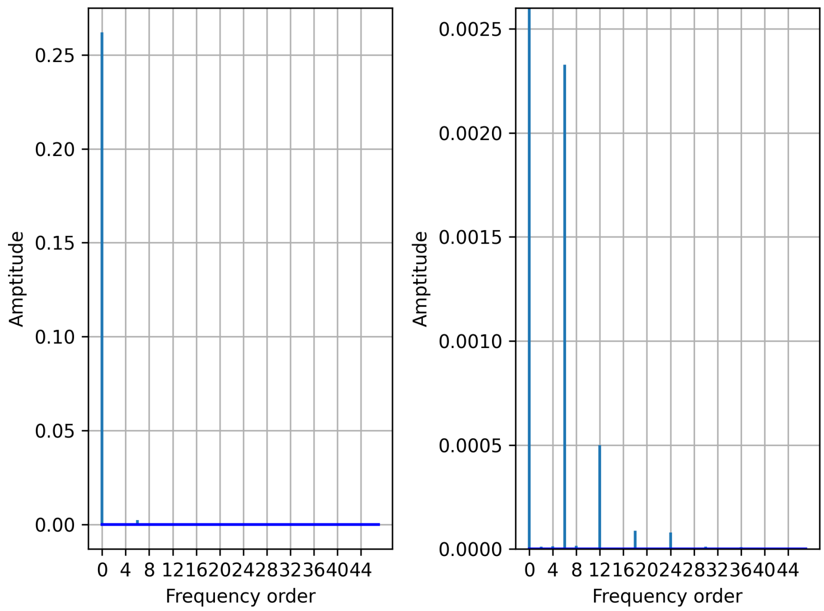

Figure 2.14: FFT for Q-axis flux with high resolution and its zoom in

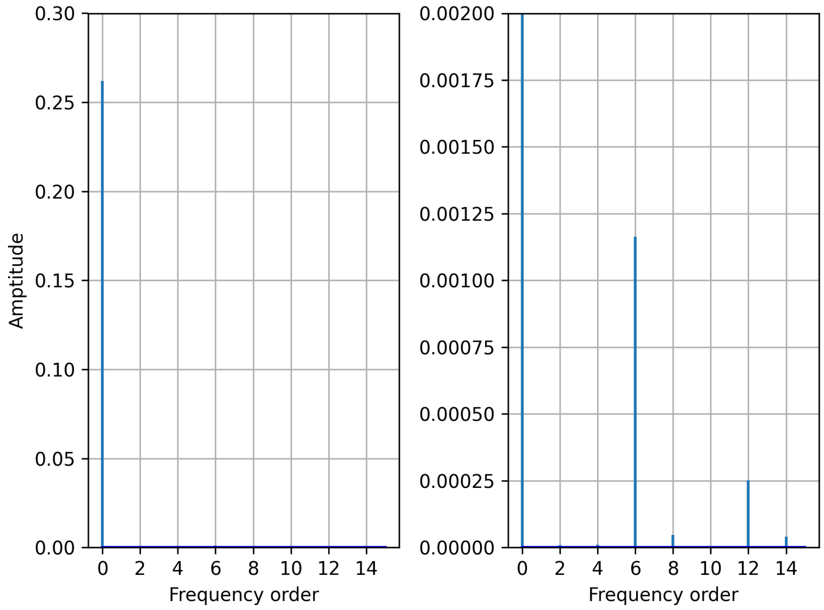

Figure 2.15: FFT for Q-axis flux with low resolution and its zoom in

Figure 2.16 and 2.17 show that torque has a dominating 6th and also 12th harmonics, resulting from the flux harmonics. There is little difference for the magnitude of the fundamental, the 6th and the 12th between the FFT results with low resolution and high resolution.

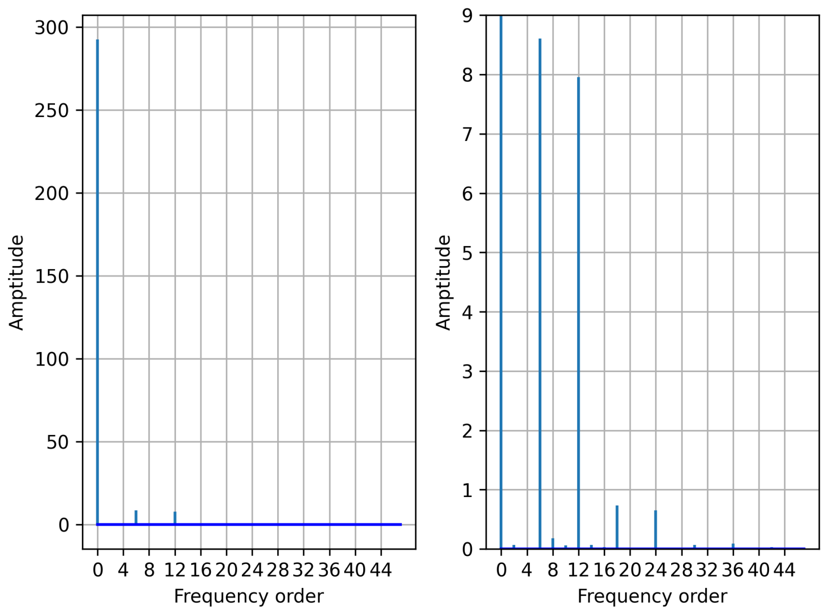

Figure 2.16: FFT for torque with high resolution and its zoom in

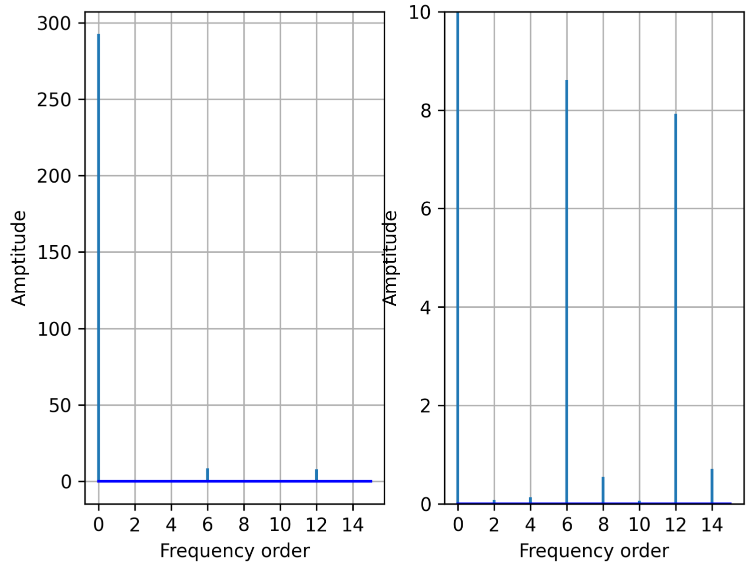

Figure 2.17: FFT for torque with low resolution, and its zoom in

2.5.3 Spatial harmonics at different operating points

It's also meaningful to investigate the 6th and 12th spatial harmonics magnitude percentage of the fundamental magnet at different operating points, to understand their distribution characteristics. Figure 2.18 and 2.19 show the 6th and 12th harmonics contour for d-axis flux.

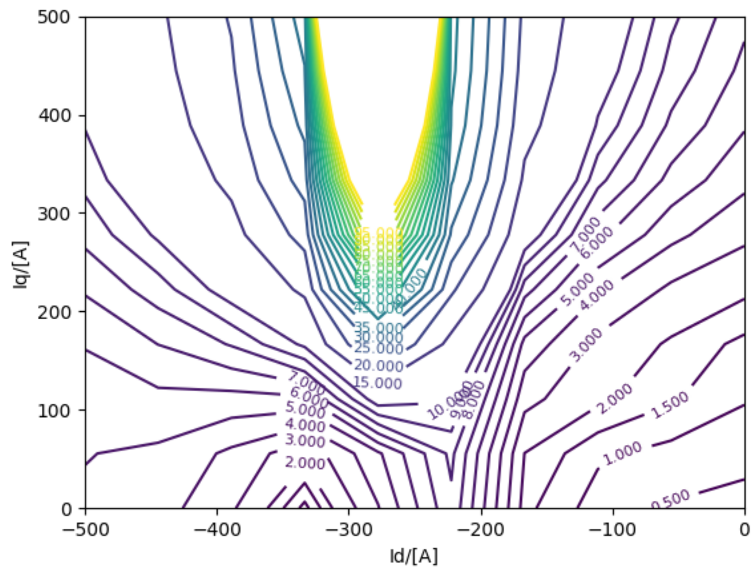

Figure 2.18: The percentage for d-axis flux 6th harmonic magnitude of the fundamental amplitude for different operating points in %

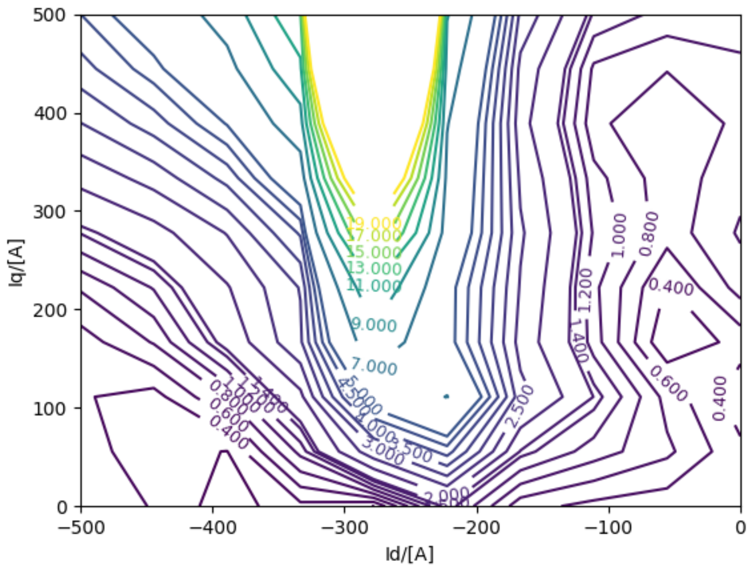

Figure 2.19: The percentage for d-axis flux 12th harmonic magnitude of the fundamental amplitude for different operating points in %

Figure 2.20 and 2.21 shows the 6th and 12th harmonics contour for q-axis flux.

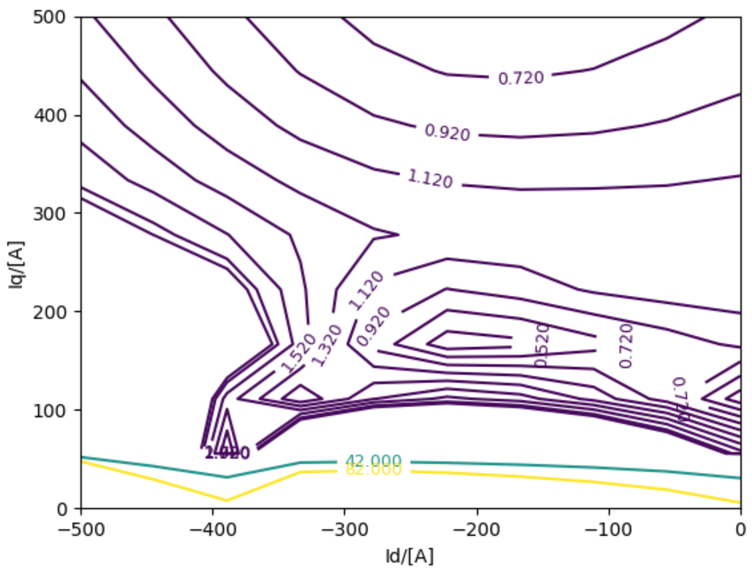

Figure 2.20: The percentage for q-axis flux 6th harmonic magnitude of the fundamental amplitude for different operating points in %

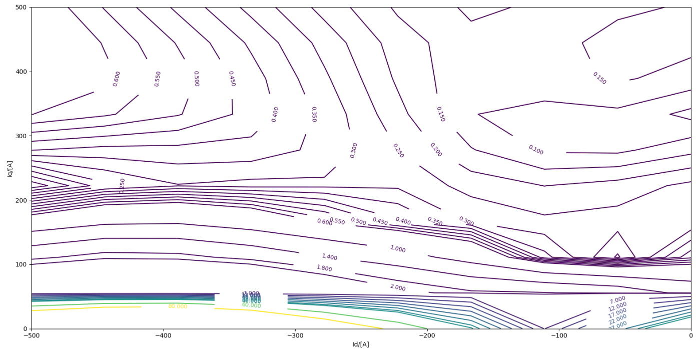

Figure 2.21: The percentage for q-axis flux 12th harmonic magnitude of the fundamental amplitude for different operating points in %

Figure 2.22 and 2.23 show the torque 6th harmonic magnitude and its percentage of the fundamental of the fundamental torque. Most of the torque harmonic magnitude percentage is between $1\% - 2\%$. It can be neglected for the region with a percentage more than 10% for the base torque magnitude is close to zero so the percentage isn't accurate. The figures show the possibility to select an operating region with a smaller torque ripple harmonic magnitude, which, however, will be at the expense of the higher stator winding losses due to the deviation from the MTPA operation.

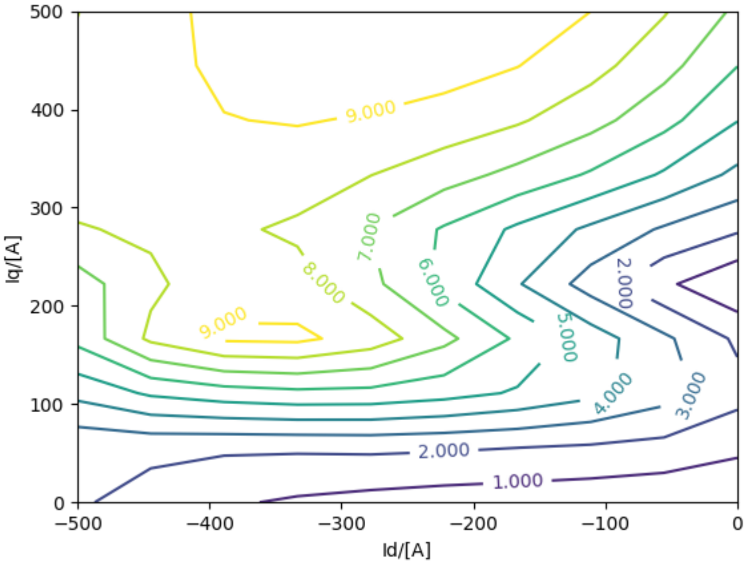

Figure 2.22: Torque 6th harmonic magnitude for different operating points /[Nm]

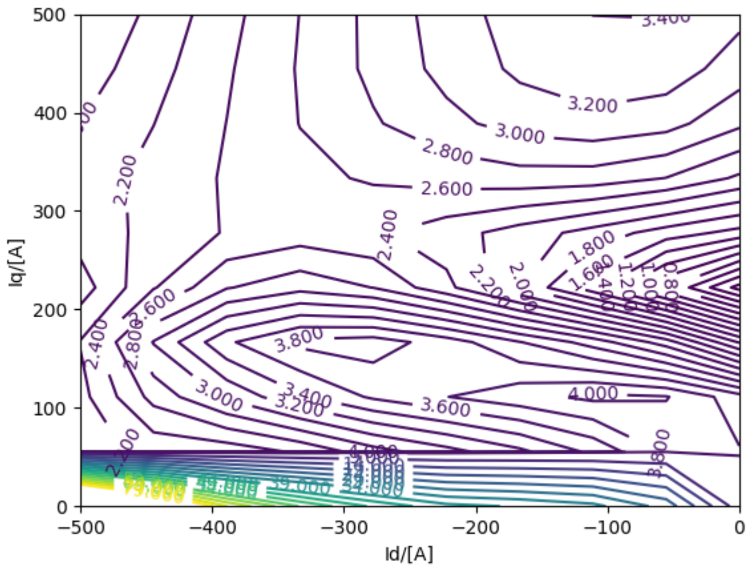

Figure 2.23: The percentage for torque 6th harmonic magnitude of the fundamental amplitude for different operating points in %

Figure 2.24 and 2.25 show torque 12th harmonic magnitude and its percentage of the fundamental of the fundamental torque. Most of the torque harmonic magnitude percentage is between $1\% - 4\%$ and the region with a percentage of more than 10% is the also neglected.

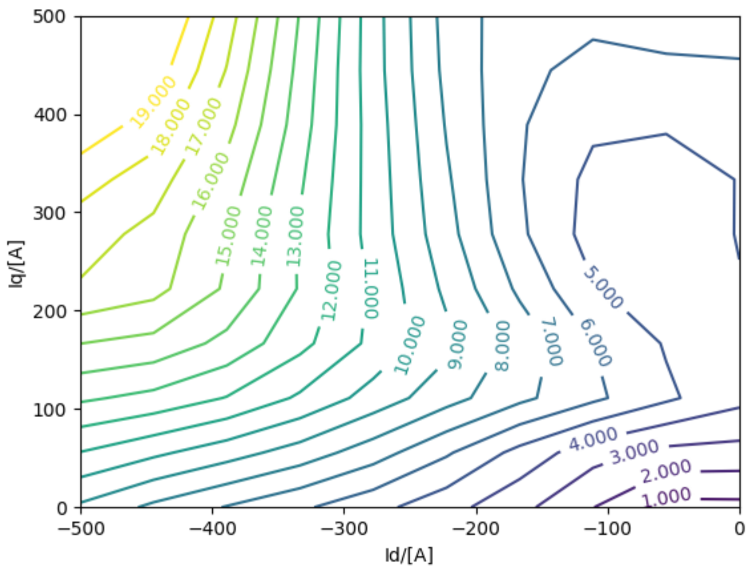

Figure 2.24: Torque 12th harmonic magnitude for different operating points /[Nm]

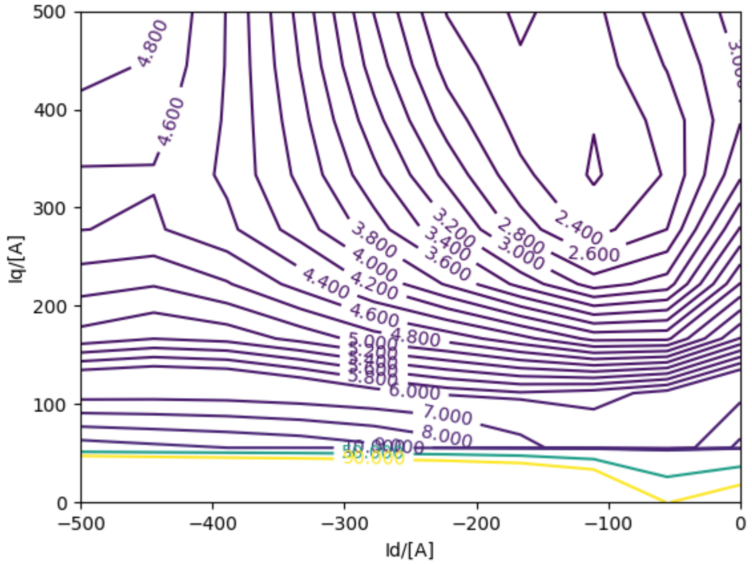

Figure 2.25: The percentage for torque 12th harmonic magnitude of the fundamental amplitude for different operating points in %

2.5.4 Look-up table generation

In this section, the obtained data list will be transferred to a Simulink lookup table using a given table generating Python package. This package can generate lookup tables of Maximum Torque per ampere(MTPA) control and the plant model. To utilize this package, all the FEM output data should be transferred into a specific Excel form. The output data is first coded to a four-dimensional array, which are d-current, q-current, temperature and rotor position. Then each dimension is exported to Excel using the Python Pandas package. Specifically, dq-currents are stored in Excel rows and columns; temperatures are stored in Excel sheets; rotor positions are stored in different Excel files.

The MTPA algorithm generates the maximum torque for a given dq current combination. Its look-up table takes in the torque reference and the available flux, and outputs the desired dq reference current. It's realized by optimising the minimum torque for each current and available flux combination, where flux is evaluated by speed.

2.6 Summary and discussions

This chapter develops the PMSM model considering saturation and spatial harmonics, through the FEM based on PYLEECAN and lookup table generation. This high fidelity plant model is vital for evaluating and improving the drive control system in Simulink in the next step.

There is a trade-off between model accuracy and FEM complicity in this thesis. A higher accuracy requires more data in current and rotor position sweeping, which causes higher calculation burden and time cost. This thesis chooses 100 current references, 96 rotor positions and 3 temperatures, which provides enough accuracy with acceptable cost.

3

Electric drive system performances with FEM plant models

In this chapter, the plant model developed in the previous chapter is applied in a PMSM electric drive system. The influence of the new plant model on the control performances with the existing control system is studied.

3.1 Overview of electric drive system

The existing drive system utilizes the field orientation control(FOC) structure as in Figure 3.1. Torque references are fed to the torque controller and corresponding current references are generated by MTPA, which has a PI controller with an active damping and anti-saturation algorithm.

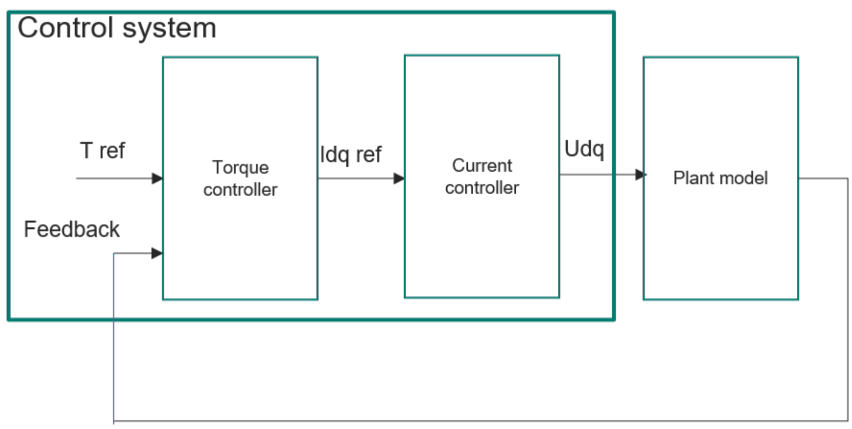

Figure 3.1: FOC scheme

The MTPA control algorithm is widely used in the electric machine control since it minimizes the stator resistive losses. The MTPA outputs the dq-axis current reference to generate the minimum stator current magnitude for a given torque reference input.

Given the PMSM parameters L_d, L_q, Ψ_m, the torque T_e can be expressed by i_d, i_q

and current angle β as

$$T_e = \frac{3n_p}{2}\Psi_m I_{mag} sin(\beta) + (L_d - L_q) I_{mag}^2 sin(\beta) cos(\beta) \tag{3.1}$$

where I_{mag} is the current magnitude. The optimum current angle β_{op} can be obtained by making the first order derivative of maximum torque to zero, assuming the inductances to be constant.

The MTPA can also be obtained using the optimization functions in MATLAB and Python, by considering the variations of the inductances. The object function is the magnitude of stator current. The inequalities constrains are the voltage and current limits.

3.2 Case setup

The simulation scenario is set up with a machine acceleration process with only its inertial limiting the speed. The torque reference steps from 0 to 200Nm at the time of 0 second. The machine speed is rised from 0 to 447 rpm in a 0.2 second time duration.

3.3 Control performance for plant model without rotor sweeping

As shown in Figure 3.2, the torque waveform doesn't have any harmonics. As Figure 3.3 indicates, there is a 1.1% deviation from the reference. The possible reason could be the inaccuracy of the plant model, caused by the trade-off between the FEM simulation cost and the accuracy.

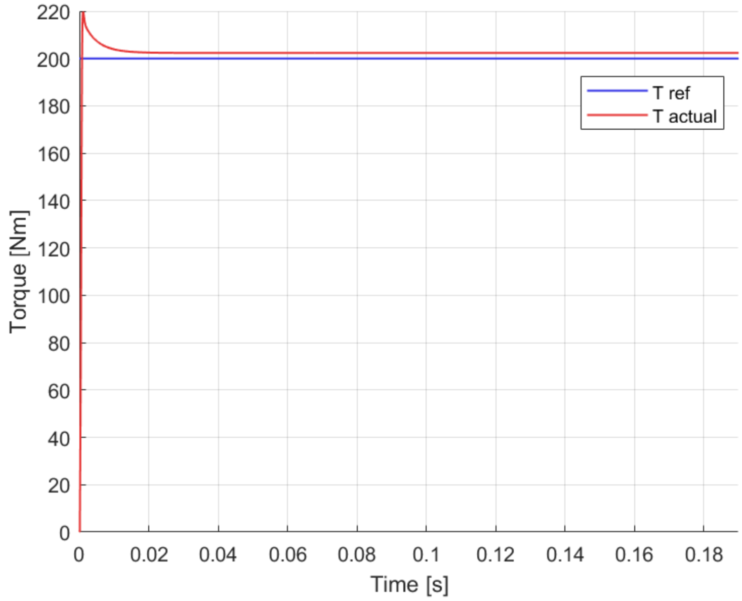

Figure 3.2: Torque waveform in the existing electric drive system

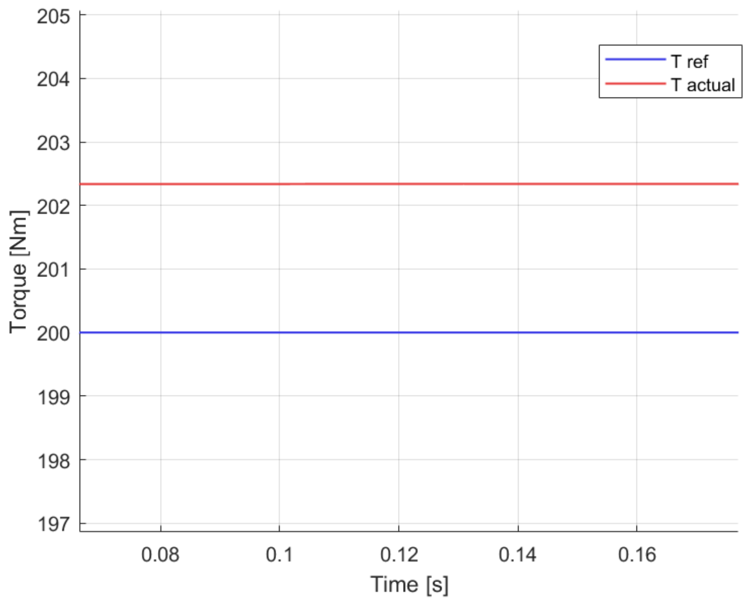

Figure 3.3: A zoom in of the torque waveform

3.4 Control performance for model with rotor sweeping

In this step, the rotor position is added as the third dimension of the current to flux lookup table. The sweeping of the rotor introduces the flux harmonics into the plant model and thus brings ripples into the torque. The The torque result is shown in Figure 3.4 and 3.5. The torque harmonics are observed with a frequency of $86.4Hz$ at the speed of 289rpm. The harmonic frequency indicates that the 6th order harmonic is dominating. The harmonic amplitude is $11.8N$, which is 3.75% of the torque fundamental magnitude. The harmonics will cause vibrations at low speed.

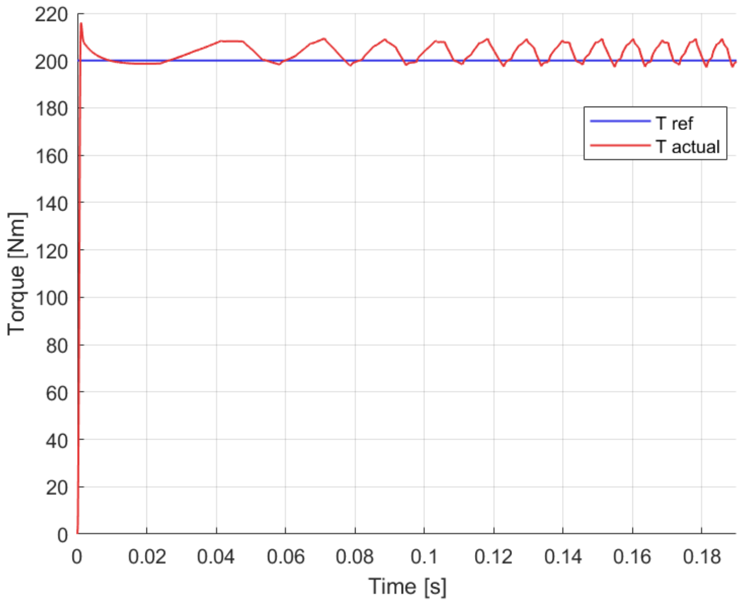

Figure 3.4: Torque waveform with the harmonics

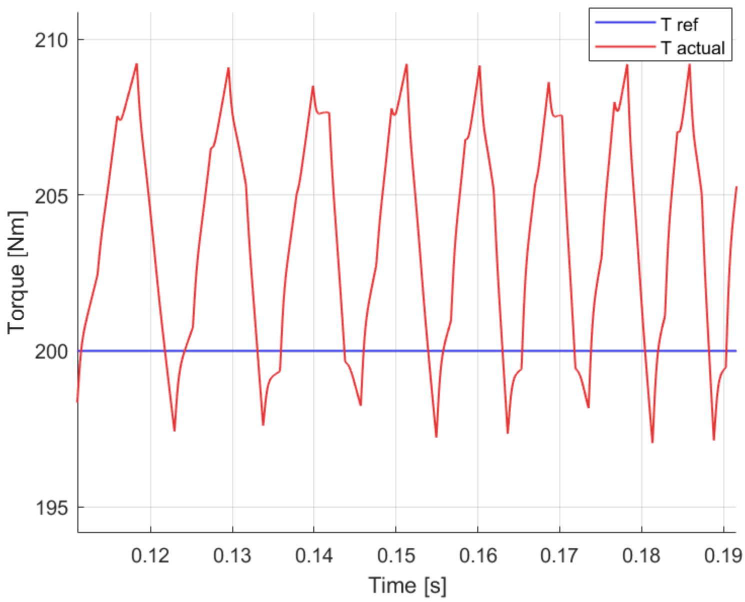

Figure 3.5: A zoom in of torque ripples

3.5 FEM Torque comparison and discussions

In this step, the torque is calculated from a 3-D lookup table from the FEM simulation instead of the torque equation in the last section. Figure 3.6 compares the torque waveform generated from the FEM lookup table and the one from the equation calculation in (2.8). The cogging torque is introduced from the FEM simulation and the cogging torque dominant frequency is the 12th according to the waveform.

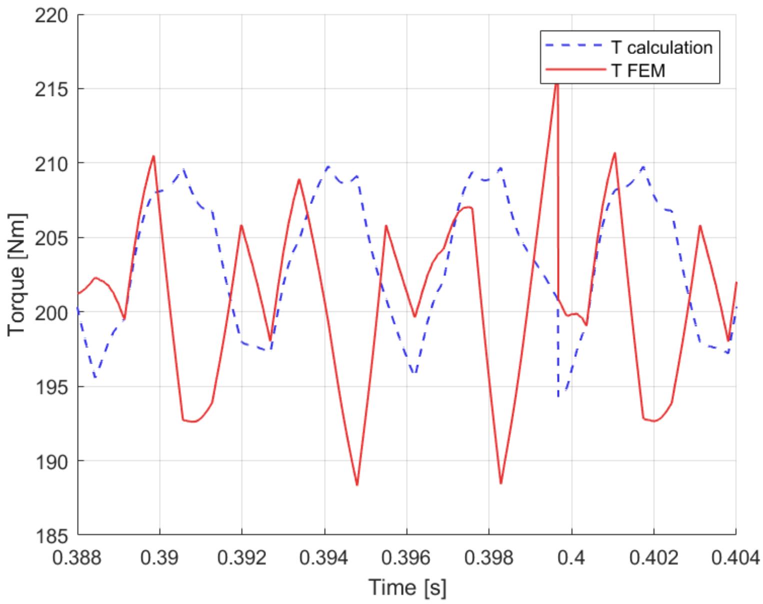

Figure 3.6: Torque waveform comparison between the FEM lookup table and the equation calculation

3.6 Torque harmonics mapping with MTPA operation

Figure 3.7 and 3.8 show the 6th and 12th torque harmonic magnitudes in the percentage of the fundamental torque magnitude. Fifty different torque-speed points are selected and the MTPA control is performed in Simulink. The torque is increased from $20Nm$ to the maximum torque of $324Nm$ with a step of $31.4Nm$. The speed is increased from $300rpm$ to $8000rpm$ with a step of $1540rpm$. At each torque-speed point, the torque is stored from the simulation results and an FFT is performed to obtain the 6th and 12th torque harmonic magnitudes.

As the harmonic mapping indicates, the torque harmonics is varied for different torque-speed situations. The 6th harmonic magnitudes exhibit lower values in the field-weakening region with the percentage value of 1%. The higher 6th harmonic magnitudes show up near the base point and the torques below $50Nm$. The 12th harmonic has lower magnitudes before the speed reaches the base point, and it becomes larger as the speed increases and the torque decreases.

The MTPA control algorithm produces the current references i_d, i_q with the specific torque-speed condition. The generated i_d, i_q map illustrates the torque harmonic magnitudes as suggested from the FEM simulation results.

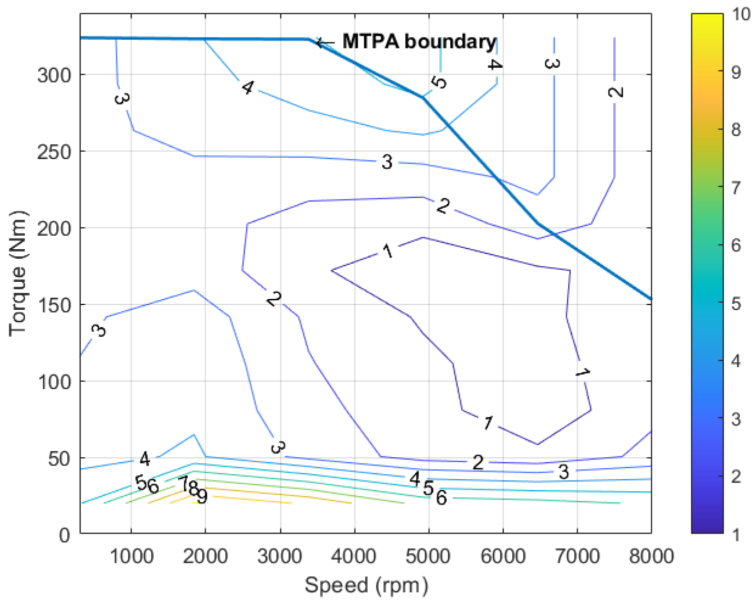

Figure 3.7: Torque 6th harmonic magnitude mapping operating in MTPA in %

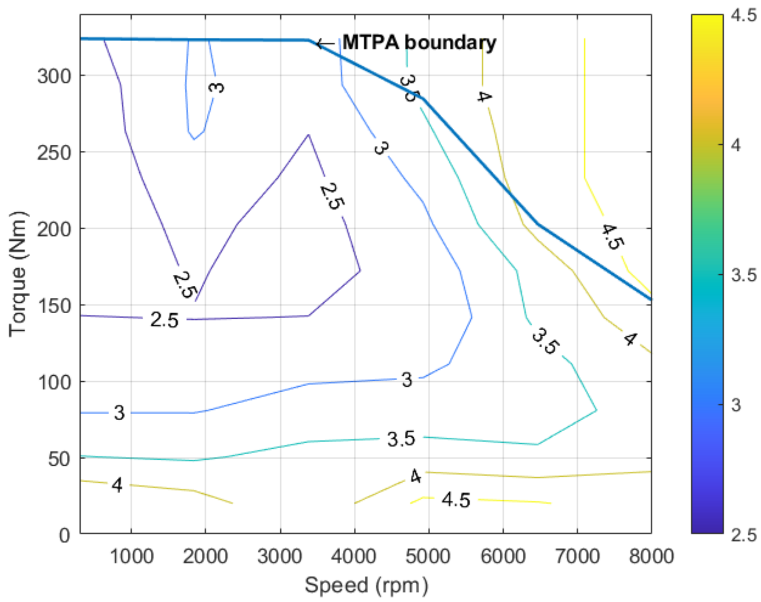

Figure 3.8: Torque 12th harmonic magnitude mapping operating in MTPA in %

3.7 Summary

When applying a model at a fixed rotor position, the existing drive system can trace the torque reference with an acceptable error. After varying the rotor positions, however, the 6th torque harmonics appear and cause problems at low speed. Thus, a compensation method is needed and will be discussed in the next chapter.

4
Compensation method

There are many proposed compensation methods as introduced in the literature review. In this thesis, the superposition principle is adopted and a compensation torque reference is added additionally in opposite phase with torque harmonics.

The compensation control scheme is shown in Figure 4.1. The acceleration is used as feedback and is fed to a high-pass filter to get the ripples. Then the ripples are fed to a PI controller and the outputs are added with the desired torque reference T ref to generate the compensated reference T_{comp}.

The feedback acceleration a_w is expressed as

$$a_w = n_p \frac{(T_{e,DC} + T_{e,har}) - T_{load}}{J} \tag{4.1}$$

where $T_{e,DC}$ is the torque DC component, $T_{e,har}$ is the torque harmonic component, T_{load} is the load torque, J is the inertia of the machine, and n_p is the machine pole pair number. The torque ripples can be obtained from the harmonics in the acceleration. Thus, a first order high-pass filter is utilized, which is realized by a transfer function as

$$H_{LP}(s) = \frac{s}{s + \omega_0} \tag{4.2}$$

where ω_0 is the cut-off frequency. The cut-off frequency is selected according to the machine speed and the estimated torque harmonic frequency.

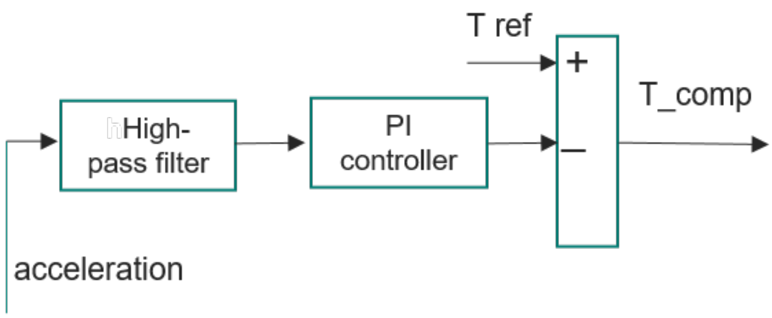

Figure 4.1: Compensation scheme

The PI controller parameters are tuned by first settling K_i fixed and tuning K_p; then K_i is tuned for a specific K_p. Enlarging K_p will better compensate for the intrinsic machine ripples; but a too high K_p value will worsen the ripple since the harmonic reference introduced will become dominating and cause additional harmonics. K_i also helps compensate but using a too high value will slower the rise time. The compensation result is shown in Figure 4.2 and 4.3.

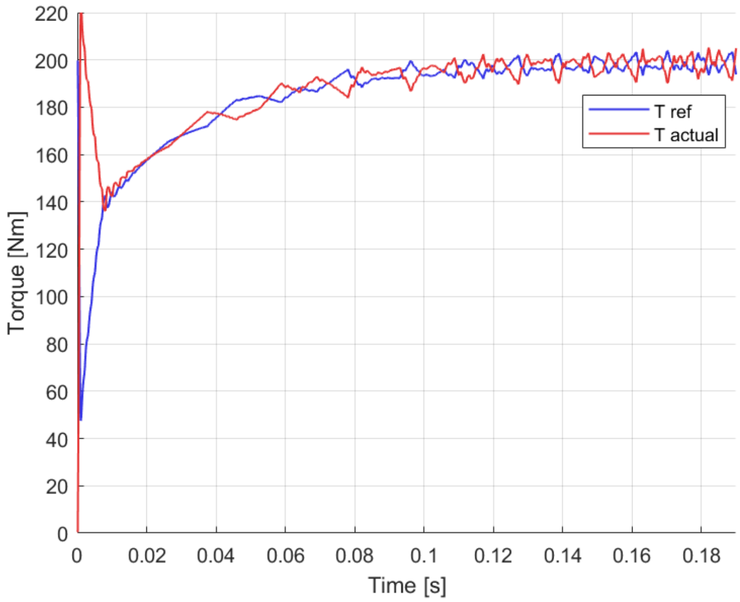

Figure 4.2: Torque result in electric drive system

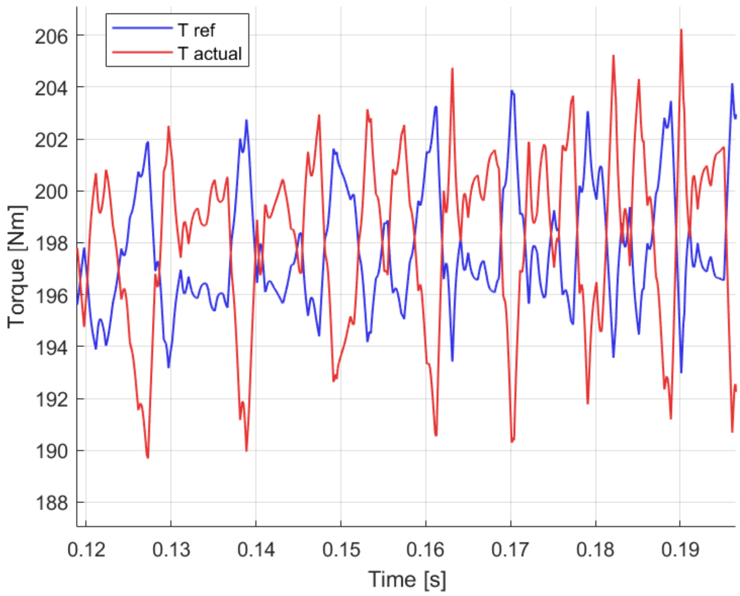

Figure 4.3: Torque result in electric drive system

It could be seen that the 6th order harmonics peaks are compensated from $20.1N$ to $14.3N$ at a speed of $289rpm$. A drawback is that the torque rise time is prolonged due to compensation and some higher harmonics are introduced by the compensated harmonics in the reference. The feedback signal can also take the machine speed depended on the application.

5

Conclusion and Discussions

5.1 Conclusion

This thesis develops a more accurate PMSM model containing spatial harmonics based on FEM and PYLEECAN. The model exports pre-calculated values to look-up table in Simulink to evaluate the existing electric drive system. The new model introduces additional torque harmonics of the dominant 6th and the 12th order. Then a compensation method is implemented to reduce the harmonics.

A programming based FEM approach is developed for the PMSM modelling to take the PMSM torque harmonics into consideration. The python programming language is adopted to define the machine dimensions and materials as well as the input current and rotor position sweeping. The fluxes and torque are obtained with different input current combinations and the results are post-processed.

Two different resolutions of the FEM simulations are used and the results are compared at a same current operation point. The results in the time domain show that the low resolution FEM simulation misses some peak ripple data compared to the high resolution FEM simulation. From the FFT analysis in the frequency domain, the torque magnitude differences between high and low resolutions are 0.03% and 0.3% for the 6th and 12th torque harmonic respectively. The high resolution results also contain the higher order harmonic information like 18th and 24th.

The look up tables are generated from the FEM results to import to Simulink. The FEM results are first converted to Excel files. Each Excel file stores the fluxes and torque data for all the input current operation points at one rotor angle position. A list of Excels store the data at different rotor positions. Then the fluxes to currents lookup tables are extracted from the Excel lists. An optimization algorithm is also performed based on the Excel data to obtain the MPTA control lookup table.

It's also feasible to develop a torque ripple compensation algorithm based on the developed PMSM plant model and the FOC drive system. The superposition principle is applied to generate the compensation torque. The simulation results show that 28.9% of the torque ripples are compensated.

5.2 Future work

Due to the time and scope limitation, some more works can be improved in the future. The machine could be directly import from .dxf file in PYLEECAN. The PMSM model with spatial harmonics can be more accurate by applying smaller current steps. More sophisticated compensation methods can be applied for the better control performances. The feedback signal in compensation can also be replaced by speed to correspond to speed sensor.

5.3 Sustainability and ethics

The European Union has proposed a 2050 long-term strategy to achieve climate-neutral without greenhouse gas emission by 2050. Developing electric vehicles is a good way to realize this target. PMSMs play an important role and become at the top of ac motors in the electric vehicle market.

The traditional combustion vehicles emit greenhouse gases and do harm to the global climate system. The development of electric vehicles can help in improving the air quality in cities by producing less carbon dioxide emissions. The popularization of electric vehicles can also help improving the environment by replacing the fossil petroleum to the sustainable resources. Electric vehicles reduce air pollution more during the driving lifetime although the extraction of the rare-earth magnets can cause some pollution in the mining.

This thesis develops a high fidelity PMSM plant model to analyze the torque ripple phenomenon. Based on the model, a straightforward compensation strategy is applied to counteract the ripples. The reduction of ripples help to increase the energy efficiency and lifetime of the PMSMs. Lower torque ripples also help to improve the EVs' drivability and the user experience for drivers. It encourages consumers to support EV and hybrid vehicles and a brings a more prosper EV market.

The code of ethics have been kept in mind while carrying out the thesis. It's important to be honest for the data and figures delivered, such as the FEM simulation results of PMSM torque and flux data. The confidentiality is also undertaken for specific information that Volvo GTT requires. For example, the given PMSM model dimension data and the given Python packages need to be kept confidential. Acknowledgement are also given to all who have offered help to the thesis.

Bibliography

[1] A. Mora, Orellana, J. Juliet, and R. Cárdenas, "Model predictive torque control for torque ripple compensation in variable-speed pmsms," *IEEE Transactions on Industrial Electronics*, vol. 63, no. 7, pp. 4584–4592, 2016.

[2] D. Wang, X. Wang, and S. Jung, "Cogging torque minimization and torque ripple suppression in surface-mounted permanent magnet synchronous machines using different magnet widths," *IEEE Transactions on Magnetics*, vol. 49, no. 5, pp. 2295–2298, 2013.

[3] W. Q. Chu and Z. Q. Zhu, "Investigation of torque ripples in permanent magnet synchronous machines with skewing," *IEEE Transactions on Magnetics*, vol. 49, no. 3, pp. 1211–1220, 2013.

[4] M. S. Islam, S. Mir, T. Sebastian, and S. Underwood, "Design considerations of sinusoidally excited permanent-magnet machines for low-torque-ripple applications," *IEEE Transactions on Industry Applications*, vol. 41, no. 4, pp. 955–962, 2005.

[5] P. Mattavelli, L. Tubiana, and M. Zigliotto, "Torque-ripple reduction in pm synchronous motor drives using repetitive current control," *IEEE Transactions on Power Electronics*, vol. 20, no. 6, pp. 1423–1431, 2005.

[6] H. Shang, L. Zhao, and T. Wang, "Torque ripple reduction for permanent magnet synchronous motor based on learning control," in *2015 2nd International Conference on Information Science and Control Engineering*, 2015, pp. 1001–1005.

[7] L. Springob and J. Holtz, "High-bandwidth current control for torque-ripple compensation in pm synchronous machines," *IEEE Transactions on Industrial Electronics*, vol. 45, no. 5, pp. 713–721, 1998.

[8] G. Feng, C. Lai, and N. C. Kar, "An analytical solution to optimal stator current design for pmsm torque ripple minimization with minimal machine losses," *IEEE Transactions on Industrial Electronics*, vol. 64, no. 10, pp. 7655–7665, 2017.

[9] M. A. Amirian, A. Rashidi, S. M. Saghaeian Nejad, and M. Mojiri, "Multiple reference frame control of permanent magnet synchronous motor with non-sinusoidal back emf using adaptive notch filter," in *2015 23rd Iranian Conference on Electrical Engineering*, 2015, pp. 1480–1485.

[10] T. Pajchrowski, "Application of neural networks for compensation of torque ripple in high performance pmsm motor," in *2017 19th European Conference on Power Electronics and Applications (EPE'17 ECCE Europe)*, 2017, pp. P.1–P.8.

[11] D. Meeker, “Finite element method magnetics.” [Online]. Available: https://www.femm.info/wiki/HomePage
[12] G. F. C. (GFC), “Pyleecan.” [Online]. Available: https://www.pyleecan.org/
[13] A. Inc, “Anaconda.” [Online]. Available: https://www.anaconda.com/
[14] R. Andersson, “On the design of electric traction machines: Design and analysis of an interior permanent magnet synchronous machine for heavy commercial vehicles,” Ph.D. dissertation, Department of Biomedical Engineering, Lund university, 2019.
[15] V. G. . C. KG, “Ndfeb magnets made of vacodym.” [Online]. Available: https://vacuumschmelze.com/products/Permanent-Magnets/NdFeB-Magnets---VACODYM

DEPARTMENT OF SOME SUBJECT OR TECHNOLOGY
CHALMERS UNIVERSITY OF TECHNOLOGY
Gothenburg, Sweden
www.chalmers.se

CHALMERS
UNIVERSITY OF TECHNOLOGY